Gain and noise in subthreshold longitudinal laser modes

R. Loudon and C. J. Shackleton
Department of Physics, University of Essex, Colchester CO4 3SQ, United Kingdom

M. Harris, T. J. Shepherd, and J. M. Vaughan
Defence Research Agency, St. Andrews Road, Malvern, Worcestershire WR14 3PS, United Kingdom
(Received 14 December 1993)

A theoretical study is presented of the gain profile and noise spectrum in the vicinity of the longitudinal-mode frequency separation of a single-mode laser amplifier of class *A* or class *B*. The gain and the noise are associated with the adjacent subthreshold modes on either side of the lasing mode; coupled equations of motion for these three modes have been solved. The amplitudes of the contributions of each individual subthreshold mode to both the gain and the noise are generally anticorrelated. Thus striking cancellation effects should occur in self-heterodyne measurements from the superposition of these contributions. The theoretical predictions are compared with the results of a parallel experimental study on a single-mode argon-ion laser amplifier. Measurements of the gain profiles and noise spectra close to the longitudinal-mode separation are reported for a range of laser output powers. Results are presented for simultaneous detection of the contributions of the two adjacent modes; for detection of only one adjacent mode, the other being suppressed with a Fabry-Pérot étalon; and again for detection of both modes but with their phase relative to the central laser beam modified by a Fabry-Pérot phase shifter. The predicted cancellation effects are clearly confirmed, and the gain profiles and noise spectra are in good agreement with the theoretical expressions. The noise-cancellation effect is demonstrated by the generation of an optical "antinoise" beam that is nearly 180° out of phase with respect to a broadband noisy input beam.

PACS number(s): 42.60.Lh, 42.60.Mi, 42.79.Qx

I. INTRODUCTION

In a recent series of papers, we have reported experimental and theoretical studies of the gain profile and intensity-fluctuation noise spectrum of the Ar^+ laser in conditions where only one longitudinal (axial) mode is above threshold [1,2]. In such experiments, it is convenient to consider the noise as arising from the beating (or heterodyning) between the broadband spontaneous noise contribution and the lasing mode. The light emitted into this mode may be considered monochromatic, and it similarly acts as the local oscillator for the gain measurements. We have shown that both the gain and the noise are controlled by previously unexplored correlations between "signal" and "image" frequency components that lie symmetrically on either side of the laser frequency. The frequency components are coupled by a four-wave-mixing process driven by pulsations in the population inversion. The effect of these correlations is generally a reduction in the gain and the noise that would be observed in their absence, so that the overall effect is one of anticorrelation.

The details of the anticorrelation between signal and image contributions should ideally be determined by experiments in which the two components are measured separately and in combination. Such experiments are difficult to perform on the single longitudinal mode of the Ar^+ laser because the narrowness of the line precludes practical separation of contributions from opposite sides of the peak. We have found, however, that the fundamental anticorrelation effects survive in the contributions to laser amplifier gain and noise from the pair of adjacent longitudinal modes on either side of the laser line. The same four-wave-mixing process via population-inversion pulsations couples the gain and the noise contributions from the adjacent modes, and the separation between longitudinal-mode frequencies is sufficiently large for relatively straightforward experimental discrimination of their contributions.

The main purpose of the present paper is a comprehensive account of the theory and experiments on adjacent longitudinal-mode gain and noise. There has been a considerable amount of previous work on laser systems that involve the excitation of two or three longitudinal modes, including studies of mode locking and competition [3–5], mode hopping [6,7], multimode instabilities [6,8], and schemes for quantum noise reduction [8,9]. Semiconductor lasers display a range of phenomena that parallel those found in gas lasers considered here. Thus a four-wave-mixing process driven by pulsations in the carrier density plays important roles in determining the relative gains of adjacent modes [10,11] and the conditions for multimode or single-mode operation [12–15]. However, the details of these effects in semiconductor lasers often differ qualitatively on account of the gain-dependent modulation of the carrier contribution to the linear refractive index (the linewidth enhancement factor), which is insignificant in gas lasers. These earlier studies of semiconductor and other varieties of laser have apparently not covered the results reported in the present paper.

Measurements of the noise spectra in the vicinity of the longitudinal modes adjacent to the lasing modes of semiconductor lasers [16,17] have been interpreted [17] in terms of the theory for the gain presented here; this has appeared previously along with other aspects of our work in brief papers [7,18,19].

Figure 1 shows the relevant part of the longitudinal-mode structure, with a lasing mode of frequency ω_L and the adjacent modes at separation Δ on either side. The single lasing mode is selected by an intracavity étalon with the transmission characteristics indicated, so that the additional loss at the adjacent modes is sufficient to keep them below threshold. Part (a) of Fig. 1 represents the two noise contributions from the adjacent modes, which we shall find to be anticorrelated to an extent that varies not only with the values of atomic and laser parameters, but also with the laser output power. Part (b) of the figure represents the single noise contribution that can be observed with appropriate filtering of the other adjacent mode.

In addition to the longitudinal modes shown in Fig. 1 (assumed to be TEM_{00}), there are also higher-order transverse modes of the laser cavity. These lie on the high-frequency side of each longitudinal mode with offsets that range upwards from about 25 MHz with increasingly complicated transverse intensity distribution. These transverse modes also show interesting gain and noise properties [20,21], but their behavior differs somewhat from that of the family of longitudinal modes with lowest-order transverse properties, i.e., that which contains the lasing mode. Because of their different transverse distributions, they tend to interact with different spatial parts of the gain medium and their dynamics are partially decoupled from those of the lowest-order transverse modes. Also, because a higher-order transverse mode has in general no image mode on the opposite side of the laser frequency ω_L, there is no enhancement of the population-inversion-driven four-wave-mixing process, and the anticorrelation effect cannot develop. We therefore do not include transverse modes other than TEM_{00} in the present account.

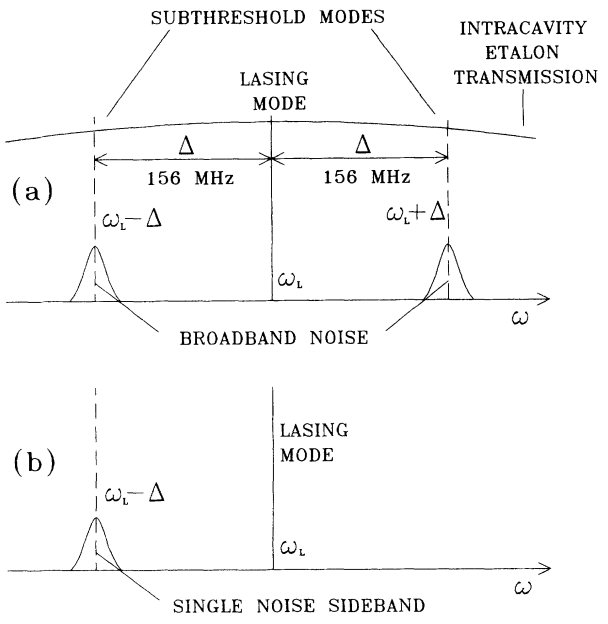

FIG. 1. (a) Position of the lasing mode, subthreshold modes, and intracavity étalon transmission. (b) Spectrum of the beam for single-sideband intensity-fluctuation measurements.

The theory of the gain and the noise associated with the adjacent subthreshold modes is presented in Sec. II. The calculations are an extension of the analysis previously presented [2] for the gain and the noise at frequencies within the central laser mode, where it is now necessary to include the contributions of the three distinct cavity modes represented in Fig. 1. The Ar^+ laser used in our measurements has an atomic dipole decay rate $\gamma_\perp$ that exceeds the mode spacing Δ by a factor of order 60. The laser gain is therefore constant over the frequency range $\omega_L-\Delta$ to $\omega_L+\Delta$ of interest here. Thus the effects of any inhomogeneous broadening can be neglected, and the motion of the atomic dipole moment can be decoupled adiabatically from the other laser variables. The other atomic variable, which describes the population inversion, has a decay rate $\gamma_\parallel$ whose magnitude is comparable to the mode spacing Δ. It is therefore necessary to seek solutions of the coupled equations of motion for the population inversion and the cavity fields. The Ar^+ laser is normally assigned to class A, specified by the condition $\gamma_\perp \gg \gamma_\parallel \gg \gamma_c$, where γ_c is the cavity mode decay rate. We have suggested [7] that a laser whose parameters satisfy this condition should quality for a subclass $A2$ and that promotion to subclass $A1$ should be granted when the more stringent condition $\gamma_\perp \gg \gamma_\parallel \gg \Delta$ is satisfied. With the parameter values mentioned above, the Ar^+ laser clearly belongs to class $A2$. The theory presented in Sec. II also applies to class-B lasers—for example, the CO_2 laser, where the decay rates satisfy $\gamma_\perp \gg \gamma_\parallel \approx \gamma_c$.

The experimental results of measurements of subthreshold mode gain and noise for the Ar^+ laser are presented in Sec. III. The measurements cover experiments made with both simultaneous and separate detection of the contributions of the two adjacent modes, and they therefore allow a direct evaluation of the effects of anticorrelations between the mode excitations. Further experiments have been carried out in which the relative phases of the three components (signal, image, and lasing) are examined in detail. The artificial production of two anticorrelated noise sidebands has also been demonstrated. The noise level in this case is shown to be very sensitive to the phases of the separate components.

II. THEORY OF SUBTHRESHOLD-MODE GAIN AND NOISE

We need to calculate the gain and the noise at frequencies detuned from the central laser line of frequency ω_L by amounts ω that are close to the longitudinal-mode spacing Δ. The required theory can be developed by an extension of our previous work on the gain and noise at frequencies within the central laser mode [2] (this paper and its equations are identified by the abbreviation LHSV). Preliminary details of the extended theory have

been briefly reported in a previous publication [18]. We use the same notation as in these earlier papers, except that the detuning, which is here denoted ω, replaces the symbol δ used in [18]. Subscripts + and − are used to distinguish quantities that refer to the longitudinal modes adjacent to the laser mode on its high- and low-frequency sides, respectively.

In treating the gain, we consider an input signal field in the form

$$\beta_{\text{in}}=\beta_s \exp[-i(\omega_L+\omega)t] , \tag{2.1}$$

whose frequency lies within the cavity mode centered at frequency $\omega_+=\omega_L+\Delta$. Similar to the situation for a signal frequency that lies within the central laser mode, the signal excites not only the mode of frequency ω_+ but also the image mode at frequency $\omega_-=\omega_L-\Delta$. To first order in the signal amplitude β_s, the mean field α inside the laser cavity consists of the three-mode superposition

$$\alpha=\alpha_L \exp(-i\omega_L t)+\alpha_- \exp[-i(\omega_L-\omega)t] + \alpha_+ \exp[-i(\omega_L+\omega)t] , \tag{2.2}$$

where α_L is the amplitude of the free-running laser. The atomic medium that drives the laser is described by two variables, the mean collective atomic dipole moment d, with the form

$$d=d_L \exp(-i\omega_L t)+d_- \exp[-i(\omega_L-\omega)t] + d_+ \exp[-i(\omega_L+\omega)t] , \tag{2.3}$$

and the mean population inversion D, which also has three contributions in the form

$$D=D_0+D_- \exp(i\omega t)+D_+ \exp(-i\omega t) , \tag{2.4}$$

where D_0 is the constant population inversion of the free-running laser and $D_-=D_+^*$ is of first order in the input signal amplitude. The pulsations of frequency ω in the population inversion are responsible for the four-wave-mixing process that couples the signal and image excitations.

For calculations of the noise, it is necessary to consider the fluctuations of the field and atomic variables around their mean values. The fluctuations are produced by quantum noise sources whose effects can be represented by random Langevin forces. The three laser variables each have their own Langevin force, denoted Γ_α, Γ_D, and Γ_d, but Γ_α is generally very small, and it is set equal to zero as in LHSV (2.14). The remaining forces have zero mean values,

$$\langle \Gamma_D \rangle=\langle \Gamma_d \rangle=0 , \tag{2.5}$$

as in LHSV (2.9).

The laser equations of motion are similar to LHSV (2.6) to (2.8), the conventional Maxwell-Bloch equations [4,22,23]. Thus the separated equations of motion for the three modes that make up the cavity field are

$$\dot{\alpha}_L+(\gamma_c+i\omega_L)\alpha_L=gd_L , \tag{2.6}$$

$$\dot{\alpha}_-+(\gamma_-+i\omega_-)\alpha_-=gd_- , \tag{2.7}$$

$$\dot{\alpha}_++(\gamma_++i\omega_+)\alpha_+=gd_++\gamma_c^{1/2}\beta_{\text{in}} , \tag{2.8}$$

where γ_c, γ_-, and γ_+ are the damping rates of the three field contributions, defined in the manner of LHSV (2.1) and (2.2), with the cavity here assumed to be symmetrical. The adjacent mode damping rates can generally be written

$$\gamma_\pm=\gamma_c+\epsilon_\pm , \tag{2.9}$$

where $\epsilon_\pm$ represents the extra losses in the two adjacent modes that ensure laser action only at the single mode of frequency ω_L. The forces on the right-hand sides of (2.6) to (2.8) result from the interactions of the cavity fields with the appropriate components of the collective atomic dipole moment d with coupling constant g, and the input signal β_{in} that drives the mode centered on the frequency ω_+.

The equation of motion for the atomic population inversion is identical to LHSV (2.7) in the form

$$\dot{D}+\gamma_\parallel D=\gamma_\parallel D_p-g(\alpha^* d+\alpha d^*)+\Gamma_D , \tag{2.10}$$

where the population of the lower atomic level of the laser transition is assumed to be negligible compared to that of the upper level. Here, $\gamma_\parallel$ is the population-inversion decay rate and D_p is the equilibrium population inversion in the absence of any cavity field; thus, D_p is proportional to the laser pumping rate. For the Ar^+ laser used in the measurements reported later in the paper, both natural and collisional broadening contribute to the value of the dipole decay rate, denoted $\gamma_\perp$. The corresponding homogeneous linewidth is approximately 10 GHz, and $\gamma_\perp/\Delta$ is of order 60. The laser gain is therefore flat over the frequency range ω_- to ω_+ examined here. The effect of any inhomogeneous broadening may be neglected in these conditions, and it is permissible to make an adiabatic approximation in the equation of motion for d, in the form of LHSV (2.15), putting

$$\gamma_\perp d=g\alpha D+\Gamma_d . \tag{2.11}$$

More generally, this equation is valid for lasers in classes A and B that satisfy the additional condition $\gamma_\perp \gg \Delta$, and it enables the atomic dipole moment to be removed from the equations of motion (2.6) to (2.8) and (2.10).

A. Gain

The linear amplification of the input signal is determined by solution of the Maxwell-Bloch equations (2.6) to (2.8) and (2.10), with the adiabatic approximation (2.11), where the Langevin forces are set equal to zero in the last two equations in view of the condition (2.5). With (2.11) used to eliminate d, and (2.10) separated into a dc component and a component at frequency ω, there are five equations for the five unknowns α_L, α_-, α_+, D_0, and $D_-=D_+^*$.

Two of the equations are used to obtain the parts of the solution that describe the free-running laser. Thus the mean photon number in the laser mode is given by

$$|\alpha_L|^2=(C-1)n_s , \tag{2.12}$$

where

$$C=g^2D_p/\gamma_c\gamma_\perp \tag{2.13}$$

is the cooperation parameter or normalized pumping rate, equal to unity at threshold, and

$$n_s=\gamma_\perp\gamma_\parallel/2g^2 \tag{2.14}$$

is the saturation photon number, that is, the number of photons in the laser cavity at a pumping rate equal to twice the threshold value. The solution for the steady-state population inversion is

$$D_0=\gamma_c\gamma_\perp/g^2\ , \tag{2.15}$$

independent of the pumping rate.

With the use of these solutions for $|\alpha_L|^2$ and D_0, the remaining equations of motion obtained from (2.7), (2.8), and (2.10) can be written in the forms

$$(\epsilon_-+i\omega-i\Delta)\gamma_\perp\alpha_- -g^2\alpha_L D_-=0\ , \tag{2.16}$$

$$(\epsilon_+-i\omega+i\Delta)\gamma_\perp\alpha_+ -g^2\alpha_L D_+=\gamma_\perp\gamma_c^{1/2}\beta_{\rm in}\ , \tag{2.17}$$

$$(C\gamma_\parallel-i\omega)D_+ +2\gamma_c(\alpha_L^*\alpha_+ +\alpha_L\alpha_-^*)=0\ . \tag{2.18}$$

It is convenient to take the complex conjugate of the first of these equations and to solve them for the variables α_-^*, α_+, and D_+, with the results

$$\alpha_-^*=-\gamma_\parallel\gamma_c(C-1)\gamma_c^{1/2}\beta_{\rm in}\exp(-2i\phi_L)/\mathcal{A}_{\rm den}\ , \tag{2.19}$$

$$\alpha_+=[(\epsilon_--i\omega+i\Delta)(C\gamma_\parallel-i\omega) +\gamma_\parallel\gamma_c(C-1)]\gamma_c^{1/2}\beta_{\rm in}/\mathcal{A}_{\rm den}\ , \tag{2.20}$$

$$D_+=-2\gamma_c^{3/2}\alpha_L^*\beta_{\rm in}(\epsilon_--i\omega+i\Delta)/\mathcal{A}_{\rm den}\ , \tag{2.21}$$

with a denominator

$$\mathcal{A}_{\rm den}=(\epsilon_+-i\omega+i\Delta)(\epsilon_--i\omega+i\Delta)(C\gamma_\parallel-i\omega) +\gamma_\parallel\gamma_c(C-1)(\epsilon_++\epsilon_--2i\omega+2i\Delta)\ , \tag{2.22}$$

where ϕ_L is the phase of the laser field,

$$\alpha_L=|\alpha_L|\exp(i\phi_L)\ . \tag{2.23}$$

In the experiments reported later in the paper, the additional losses ϵ_- and ϵ_+ at the adjacent modes are produced by the insertion of an intracavity étalon whose transmission maximum can be tuned through the range of frequencies covered by the three modes considered here. We have shown that complicated gain profiles and noise spectra can occur when the étalon maximum is detuned from ω_L so that ϵ_- is quite different from ϵ_+ [18]. For sufficient étalon detuning, the lasing frequency hops from ω_L to one of the adjacent modes, and we have shown that the hopping behavior displays hysteresis effects which can be understood on the basis of expressions for the gain obtained from the above calculation with $\epsilon_-\neq\epsilon_+$ [7] (see also [6]). However, the experiments reported in the present paper use a symmetrically tuned étalon with

$$\epsilon_-=\epsilon_+\equiv\epsilon\ , \tag{2.24}$$

and we henceforth make this assumption in the theory. The denominator (2.22) simplifies to

$$\mathcal{A}_{\rm den}=[(\epsilon-i\omega+i\Delta)(C\gamma_\parallel-i\omega)+2\gamma_\parallel\gamma_c(C-1)] \times(\epsilon-i\omega+i\Delta)\ . \tag{2.25}$$

Consider first a pair of experiments in which the laser output from only one of the adjacent modes, centered on either ω_- or ω_+, is observed in isolation from the other adjacent mode. The theory of gain measurements using one or both adjacent modes is outlined in the Appendix. The intensity gains in transmission obtained with the use of (2.19) and (2.20) are

$$G_{T^-}=\gamma_c\left|\frac{\alpha_-}{\beta_s}\right|^2=\frac{\gamma_\parallel^2\gamma_c^4(C-1)^2}{\mathcal{D}_{\rm den}} \tag{2.26}$$

and

$$G_{T^+}=\gamma_c\left|\frac{\alpha_+}{\beta_s}\right|^2=\frac{\gamma_c^2\{[(\omega-\Delta)C\gamma_\parallel+\epsilon\Delta]^2+[(\omega-\Delta)\Delta-\epsilon C\gamma_\parallel-\gamma_\parallel\gamma_c(C-1)]^2\}}{\mathcal{D}_{\rm den}}\ , \tag{2.27}$$

where

$$\mathcal{D}_{\rm den}=|\mathcal{A}_{\rm den}|^2 =\{[(\omega-\Delta)C\gamma_\parallel+\epsilon\Delta]^2 +[(\omega-\Delta)\Delta-\epsilon C\gamma_\parallel-2\gamma_\parallel\gamma_c(C-1)]^2\} \times[(\omega-\Delta)^2+\epsilon^2]\ . \tag{2.28}$$

In view of the proximity of the detuning ω to the mode spacing in the experiments considered here, ω has been replaced by Δ in the above expressions except where it occurs in the combination $\omega-\Delta$. The denominator can be reexpressed as a product of two Lorentzian factors:

$$\mathcal{D}_{\rm den}=(C^2\gamma_\parallel^2+\Delta^2)[(\omega-\Delta-S)^2+(\Gamma/2)^2] \times[(\omega-\Delta)^2+\epsilon^2]\ , \tag{2.29}$$

where

$$S=\frac{2\Delta\gamma_\parallel\gamma_c(C-1)}{C^2\gamma_\parallel^2+\Delta^2} \tag{2.30}$$

and

$$\Gamma=\frac{4\gamma_\parallel^2\gamma_c C(C-1)}{C^2\gamma_\parallel^2+\Delta^2}+2\epsilon\ . \tag{2.31}$$

The first Lorentzian factor shows a shift S in its resonance frequency away from the mode spacing Δ; the shift varies with laser power in the manner illustrated in Fig. 2, with zero shift at threshold ($C=1$) and at very high powers ($C\to\infty$), and a maximum value of

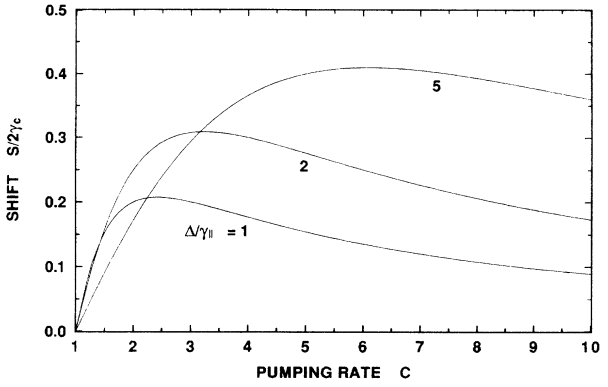

FIG. 2. Theoretical behavior of double-sideband gain and noise profiles: shift. The profiles are of Lorentzian shape throughout.

$$S_{\max}=\frac{\Delta\gamma_c}{\gamma_\parallel+(\Delta^2+\gamma_\parallel^2)^{1/2}} \tag{2.32}$$

at a power corresponding to

$$C-1=[1+(\Delta/\gamma_\parallel)^2]^{1/2} . \tag{2.33}$$

The full width at half maximum (FWHM) bandwidth Γ of the first Lorentzian factor varies with C as shown in Fig. 3; the bandwidth tends to $4\gamma_c+2\epsilon$ at high laser powers, compared to the values $2\gamma_c$ of the empty cavity bandwidth. The width and shift are simply related by

$$\frac{\Gamma-2\epsilon}{2S}=\frac{C\gamma_\parallel}{\Delta} . \tag{2.34}$$

It is of course possible in principle to separate the two gains (2.26) and (2.27) into contributions that have the individual Lorentzian denominators from (2.29), but the resulting expressions are complicated and we do not give them here.

The gains (2.26) and (2.27) are not in fact ordinarily observed in the straightforward arrangement where the laser amplifier output falls on a photodetector without any intermediate filtering. Such an experiment, as reported in Sec. III A, observes simultaneously the self-heterodyne beats between the strong laser beam of frequency ω_L and the signal and image contributions of equal and opposite detuning. Then similar to LHSV (5.15) and (5.17), and as outlined in the Appendix, the transmission gain is given by

$$G_T(\omega)=\gamma_c|(\alpha_L^*\alpha_+ +\alpha_L\alpha_-^*)/\alpha_L^*\beta_s|^2 , \tag{2.35}$$

and use of the solutions (2.19) and (2.20) for the field amplitudes gives the simple expression

$$G_T(\omega)=\frac{\gamma_c^2}{(\omega-\Delta-S)^2+(\Gamma/2)^2} , \tag{2.36}$$

where the shift S and width Γ are again given by (2.30) and (2.31), respectively. Remarkably, the gain profile is therefore a single Lorentzian, the final factor in the denominator (2.29) having cancelled in the formation of the sum of signal and image contributions in (2.35). The gain (2.36) is thus the net result from partial cancellation of larger out-of-phase amplitude gains for the individual adjacent modes. The similar cancellation that occurs for an input signal whose frequency lies within the central lasing mode is discussed by LHSV.

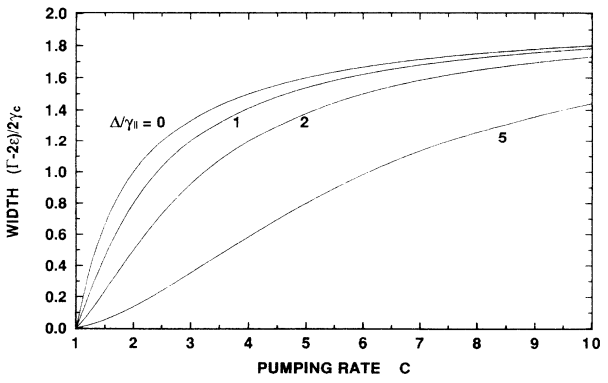

FIG. 3. Theoretical behavior of double-sideband gain and noise profiles: width.

B. Noise

We use again the Maxwell-Bloch equations (2.6) to (2.8), (2.10), and (2.11) with the forces Γ_D and Γ_d now retained but the signal amplitude β_{in} set equal to zero. We look for field solutions similar to (2.2) but with the modified form

$$\begin{aligned}\alpha(t)=&[\alpha_L+\delta\alpha_L(t)]\exp(-i\omega_L t)\\&+\delta\alpha_-(t)\exp[-i(\omega_L-\Delta)t]\\&+\delta\alpha_+(t)\exp[-i(\omega_L+\Delta)t] ,\end{aligned} \tag{2.37}$$

where the $\delta\alpha$ quantities represent zero-mean-field fluctuations associated with the three modes and only the laser mode has a nonzero mean field α_L. The population inversion is also similar to (2.4) but with the modified form

$$\begin{aligned}D(t)=&D_0+\delta D(t)+\delta D_-(t)\exp(i\Delta t)\\&+\delta D_+(t)\exp(-i\Delta t) ,\end{aligned} \tag{2.38}$$

where

$$\delta D_-(t)=\delta D_+^*(t) . \tag{2.39}$$

These trial solutions are now substituted into the Maxwell-Bloch equations and only the terms of first order in the fluctuating variables and the Langevin forces are retained. The noise properties of the central lasing mode, determined by the solutions for $\delta\alpha_L(t)$ and $\delta D(t)$, have been fully discussed by LHSV. We consider here the noise properties of the adjacent modes, determined by the solutions for $\delta\alpha_-(t)$, $\delta\alpha_+(t)$, and $\delta D_-(t)$ or $\delta D_+(t)$. The required equations of motion are

$$\begin{aligned}&\delta\dot\alpha_-(t)+\epsilon_-\delta\alpha_-(t)-(g^2/\gamma_\perp)\alpha_L\delta D_-(t)\\&\qquad=(g/\gamma_\perp)\Gamma_d(t)\exp[i(\omega_L-\Delta)t] ,\end{aligned} \tag{2.40}$$

$$\begin{aligned}&\delta\dot\alpha_+(t)+\epsilon_+\delta\alpha_+(t)-(g^2/\gamma_\perp)\alpha_L\delta D_+(t)\\&\qquad=(g/\gamma_\perp)\Gamma_d(t)\exp[i(\omega_L+\Delta)t] ,\end{aligned} \tag{2.41}$$

and

$$\delta\dot{D}_+(t)+(C\gamma_\parallel-i\Delta)\delta D_+(t)+2\gamma_c\{\alpha_L\delta\alpha_-(t)^*+\alpha_L^*\delta\alpha_+(t)\}$$
$$=-(g/\gamma_\perp)\{\alpha_L\Gamma_d^*(t)\exp(-i\omega_L t)+\alpha_L^*\Gamma_d(t)\exp(i\omega_L t)\}\exp(i\Delta t)+\Gamma_D(t)\exp(i\Delta t)\ , \quad (2.42)$$

where (2.9) and (2.12) to (2.15) have been used.

It is convenient to solve the equations of motion by taking somewhat unconventional Fourier transforms of the various time-dependent quantities defined in accordance with

$$\delta\alpha_+(\omega)=(2\pi)^{-1/2}\int dt\,\exp[i(\omega-\Delta)t]\delta\alpha_+(t)\ ,$$
$$\delta\alpha_-^*(\omega)=(2\pi)^{-1/2}\int dt\,\exp[i(\omega-\Delta)t]\delta\alpha_-^*(t)\ , \quad (2.43)$$
$$\Gamma_d(\omega)=(2\pi)^{-1/2}\int dt\,\exp[i(\omega-\Delta)t]\Gamma_d(t)\ ,$$

and so on. The Fourier transforms of (2.40) to (2.42) can then be solved straightforwardly for the three variables of interest and the results are

$$\delta\alpha_+(\omega)=((g/\gamma_\perp)\{(\epsilon-i\omega+i\Delta)[\tfrac{1}{2}\gamma_\parallel(C+1)-i\Delta]+\gamma_\parallel\gamma_c(C-1)\}\Gamma_d(\omega_L+\omega)$$
$$-(g^3/\gamma_\perp^2)(2\gamma_c+\epsilon-i\omega+i\Delta)\alpha_L^2\Gamma_d^*(\omega_L-\omega)+(g^2/\gamma_\perp)(\epsilon-i\omega+i\Delta)\alpha_L\Gamma_d(\omega))/\mathcal{A}_{\rm den}\ , \quad (2.44)$$

$$\delta\alpha_-^*(\omega)=(-(g^3/\gamma_\perp^2)(2\gamma_c+\epsilon-i\omega+i\Delta)\alpha_L^{*2}\Gamma_d(\omega_L+\omega)$$
$$+(g/\gamma_\perp)\{(\epsilon-i\omega+i\Delta)[\tfrac{1}{2}\gamma_\parallel(C+1)-i\Delta]+\gamma_\parallel\gamma_c(C-1)\}\Gamma_d^*(\omega_L-\omega)$$
$$+(g^2/\gamma_\perp)(\epsilon-i\omega+i\Delta)\alpha_L^*\Gamma_D(\omega))/\mathcal{A}_{\rm den} \quad (2.45)$$

and

$$\delta D_+(\omega)=\{-(g/\gamma_\perp)(2\gamma_c+\epsilon-i\omega+i\Delta)[\alpha_L^*\Gamma_d(\omega_L+\omega)+\alpha_L\Gamma_d^*(\omega_L-\omega)]+(\epsilon-i\omega+i\Delta)\Gamma_D(\omega)\}(\epsilon-i\omega+i\Delta)/\mathcal{A}_{\rm den}\ , \quad (2.46)$$

where the denominator is given by (2.22) and the additional losses at the adjacent modes have been assumed equal as in (2.24).

The Langevin force correlation functions that are needed to evaluate the power spectra of the field fluctuations are obtained from the results of Louisell [22]. For lasers in which $\gamma_\perp$ is very much larger than both $\gamma_\parallel$ and Δ, the only correlations of significant magnitude are given by

$$\langle\Gamma_d^*(\omega_L+\omega)\Gamma_d(\omega_L+\omega')\rangle=2\gamma_\perp D_0\delta(\omega-\omega') \quad (2.47)$$

and

$$\langle\Gamma_D(\omega)\Gamma_D^*(\omega')\rangle=2\gamma_\parallel D_0\delta(\omega-\omega')\ , \quad (2.48)$$

where the reality of $\Gamma_D(t)$ has been used. It is now algebraically tedious but straightforward to evaluate the adjacent-mode noise-field correlation functions and the results are

$$\langle\delta\alpha_-^*(\omega)\delta\alpha_-(-\omega')\rangle=\langle\delta\alpha_+^*(\omega)\delta\alpha_+(-\omega')\rangle$$
$$=\gamma_c\delta(\omega+\omega')\left\{\frac{1}{(\omega-\Delta)^2+\epsilon^2}+\frac{C\gamma_\parallel^2+\Delta^2}{C^2\gamma_\parallel^2+\Delta^2}\frac{1}{(\omega-\Delta-S)^2+(\Gamma/2)^2}\right\} \quad (2.49)$$

and

$$\langle\delta\alpha_-(\omega)\delta\alpha_+(-\omega')\rangle=\gamma_c\exp(2i\phi_L)\delta(\omega+\omega')\left\{-\frac{1}{(\omega-\Delta)^2+\epsilon^2}+\frac{C\gamma_\parallel^2+\Delta^2}{C^2\gamma_\parallel^2+\Delta^2}\frac{1}{(\omega-\Delta-S)^2+(\Gamma/2)^2}\right\}\ , \quad (2.50)$$

where the shift S and width Γ are given by (2.30) and (2.31). For reasons to be discussed, we refer to the two Lorentzians in (2.49) and (2.50) as the phase modulation (PM) and amplitude modulation (AM) components of the adjacent-mode noise spectra, respectively. It is seen from (2.50) that the AM components of the noise for the two modes have the same phase but the PM components are in antiphase.

Consider first an experiment in which the output from the laser falls on a photodetector but with the noise contribution from one of the adjacent modes removed by a filter. The arrangement is therefore analogous to the single-mode gain measurements treated in (2.26) and (2.27). The experiment observes the self-heterodyne beats between the laser light and one adjacent-mode noise component, and the spectra are proportional to the correla-

tion functions given in (2.49), as outlined in the Appendix. It is seen that the PM and AM components of the noise both contribute, analogous to the occurrence of both Lorentzian factors in the denominator (2.29) of the single-mode gains. The integrated spectra are proportional to

$$\int d\omega \int d\omega' \langle \delta\alpha_{\pm}^{*}(\omega)\delta\alpha_{\pm}(-\omega')\rangle = \pi\gamma_c \left\{ \frac{1}{\epsilon} + \frac{C\gamma_{\parallel}^2+\Delta^2}{2\gamma_{\parallel}^2\gamma_c C(C-1)+\epsilon(C^2\gamma_{\parallel}^2+\Delta^2)} \right\}, \tag{2.51}$$

where (2.31) has been used to express Γ in terms of the primary parameters of the laser model.

Now consider an experiment in which both adjacent-mode noise components and the strong laser light fall on a photodetector. Then similar to the gain measurement treated in (2.35), the self-heterodyne spectrum is proportional to the square modulus of the quantity:

$$\delta A(\omega,0)=\alpha_L\delta\alpha_{-}^{*}(\omega)+\alpha_L^{*}\delta\alpha_{+}(\omega) . \tag{2.52}$$

Experiments reported in Sec. III C make measurements of this kind but with the added feature that the phase of the laser light is shifted by an amount ϕ_E relative to that of the noise, by means of a Fabry-Pérot étalon. We thus need to consider a more general quantity,

$$\delta A(\omega,\phi_E)=\alpha_L \exp(i\phi_E)\delta\alpha_{-}^{*}(\omega) + \alpha_L^{*}\exp(-i\phi_E)\delta\alpha_{+}(\omega) , \tag{2.53}$$

and, in accordance with the argument given in the Appendix, the self-heterodyne spectrum is proportional to

$$\langle \delta A^{*}(\omega,\phi_E)\delta A(-\omega',\phi_E)\rangle/|\alpha_L|^2 = 4\gamma_c\delta(\omega+\omega') \left\{ \frac{\sin^2\phi_E}{(\omega-\Delta)^2+\epsilon^2} + \frac{C\gamma_{\parallel}^2+\Delta^2}{C^2\gamma_{\parallel}^2+\Delta^2} \frac{\cos^2\phi_E}{(\omega-\Delta-S)^2+(\Gamma/2)^2} \right\}, \tag{2.54}$$

where (2.49) and (2.50) have been used. The integrated spectrum is

$$\int d\omega \int d\omega' \langle \delta A^{*}(\omega,\phi_E)\delta A(-\omega',\phi_E)\rangle/|\alpha_L|^2 = 4\pi\gamma_c \left\{ \frac{\sin^2\phi_E}{\epsilon} + \frac{(C\gamma_{\parallel}^2+\Delta^2)\cos^2\phi_E}{2\gamma_{\parallel}^2\gamma_c C(C-1)+\epsilon(C^2\gamma_{\parallel}^2+\Delta^2)} \right\}. \tag{2.55}$$

The straightforward experiment with no additional phase shift in the laser light ($\phi_E=0$) thus observes only the AM component of the adjacent-mode noise, with four times the strength obtained in measurements of the single-mode noise, described by (2.49) and (2.51). The PM noise component is removed because of the opposite phases of the contributions of the two adjacent modes. This behavior is analogous to the occurrence of the single Lorentzian in the two-mode gain profile (2.36). Thus similar cancellation effects between the contributions of the two adjacent modes occur in both the gain profile and the noise spectrum. More generally, (2.54) and (2.55) show that arbitrary combinations of the PM and AM spectra can be observed for appropriate phase shifts ϕ_E of the laser light. Measurements of such spectra are reported in Sec. III, together with observations of single adjacent-mode noise spectra.

The detailed theory given above is complemented by a more qualitative interpretation in terms of ordinary phase and amplitude modulation [19]. Consider a carrier wave (the lasing mode) modulated by two weak sidebands of relative frequencies $\pm\omega$ and complex amplitudes $E_{\pm}(\omega)$. The total field is

$$E(t)=E_L\exp(-i\omega_L t)+E_{-}(\omega)\exp[-i(\omega_L-\omega)t] + E_{+}(\omega)\exp[-i(\omega_L+\omega)t] , \tag{2.56}$$

analogous to (2.37). We choose amplitudes and phases of the three contributions in accordance with

$$E_L=|E_L|\exp(i\phi_L) , \tag{2.57}$$

$$E_{-}(\omega)=a(\omega)\exp[i\phi_L-i\phi_{-}(\omega)] , \tag{2.58}$$

and

$$E_{+}(\omega)=a(\omega)\exp[i\phi_L-i\phi_{+}(\omega)] . \tag{2.59}$$

The real field obtained from (2.56) correct to first order in the small quantity $a(\omega)/|E_L|$ is then

$$\mathrm{Re}E(t)=\{|E_L|+2a(\omega)\cos\Phi_{-}(\omega)\cos[\omega t-\Phi_{+}(\omega)]\} \times\cos\{\omega_L t-\Phi_L-2\frac{a(\omega)}{|E_L|}\sin\Phi_{-}(\omega) \times\cos[\omega t-\Phi_{+}(\omega)]\} , \tag{2.60}$$

where

$$\Phi_{\pm}(\omega)=\tfrac{1}{2}[\phi_{+}(\omega)\pm\phi_{-}(\omega)] . \tag{2.61}$$

It is seen that the field has both phase modulation, whose depth is proportional to

$$a(\omega)\sin\Phi_{-}(\omega) \quad (\mathrm{PM}) , \tag{2.62}$$

and amplitude modulation, with depth proportional to

$$a(\omega)\cos\Phi_{-}(\omega) \quad (\mathrm{AM}) . \tag{2.63}$$

The sideband field amplitude $a(\omega)$ is assumed to be a stochastic variable whose correlation function has the form

$$\langle a(\omega)a(\omega')\rangle=\langle a^2\rangle_{\omega}\delta(\omega-\omega') , \tag{2.64}$$

where $\langle a^2\rangle_{\omega}$ is the field fluctuation power spectrum. The sideband fields (2.58) and (2.59) therefore have the corre-

lation functions

$$\langle E_+^*(\omega)E_-(-\omega')\rangle=\langle E_+^*(\omega)E_+(-\omega')\rangle$$
$$=\langle a^2\rangle_\omega\delta(\omega+\omega')\{\langle\sin^2\Phi_-(\omega)\rangle+\langle\cos^2\Phi_-(\omega)\rangle\} \quad (2.65)$$

and

$$\langle E_-(\omega)E_+(-\omega')\rangle$$
$$=\langle a^2\rangle_\omega\delta(\omega+\omega')\exp(2i\phi_L)\times\{-\langle\sin^2\Phi_-(\omega)\rangle+\langle\cos^2\Phi_-(\omega)\rangle\}\ , \quad (2.66)$$

where it is assumed that positive and negative values of $\Phi_-(\omega)$ given by (2.61) are equally likely. The large bracket in (2.65) is of course equal to unity, but the correlation function is written in this form to facilitate comparison of (2.65) and (2.66) with (2.49) and (2.50). It is seen that the following identifications of phase- and amplitude-modulation spectra can be made:

$$\langle a^2\rangle_\omega\langle\sin^2\Phi_-(\omega)\rangle=\frac{\gamma_c}{(\omega-\Delta)^2+\epsilon^2} \quad \text{(PM)} \quad (2.67)$$

and

$$\langle a^2\rangle_\omega\langle\cos^2\Phi_-(\omega)\rangle=\frac{C\gamma_\parallel^2+\Delta^2}{C^2\gamma_\parallel^2+\Delta^2}\frac{\gamma_c}{(\omega-\Delta-S)^2+(\Gamma/2)^2} \quad \text{(AM)}\ . \quad (2.68)$$

It is easily shown with the use of (2.30) and (2.31) that the two spectra become identical for $C\to 1$, with

$$\langle\cos^2\Phi_-(\omega)\rangle=\langle\sin^2\Phi_-(\omega)\rangle=\tfrac{1}{2}\ , \quad (2.69)$$

suggesting that all values of $\Phi_-(\omega)$ are equally likely. The amplitude-modulation spectrum tends to zero for $C\gg 1$, suggesting that

$$\Phi_-(\omega)=\pi/2 \ \text{ or } \ \phi_-(\omega)-\phi_+(\omega)=\pi\ , \quad (2.70)$$

with the sideband fields in antiphase.

An expression for the spectrum similar to (2.54) is obtained from the above simple model if the carrier-wave field (2.57) alone is subjected to an additional phase shift ϕ_E. In particular, the PM component of the total field (2.60) is observed with maximum strength for a carrier-wave phase shift of $\phi_E=\pi/2$. The PM component is also observed in single-sideband detection, where the measured signal is determined by the field correlation (2.65) alone. These are well-known techniques for detection of phase-modulation spectra at radio frequencies.

III. EXPERIMENTAL MEASUREMENTS OF GAIN AND NOISE

In this section we present results of gain measurements for above-threshold amplification, in which the injected signal has been tuned close to resonance with a subthreshold axial mode. The measurements are made using the same straightforward technique as in [1,18,19], and as described in detail in [2]. The technique uses an acousto-optic modulator (Fig. 4) in double pass to provide a frequency-shifted signal of variable offset ω for reinjection into the laser. The amplification is assessed from measurements of the optical beat at the detuning frequency ω. This beat results from the mixing of the output amplified signal (together with its image band counterpart) and the free-running laser output, which acts as a local oscillator. The gain is defined [1,2] as the ratio of the *measured* heterodyne beat signal power to that derived from the same input signal mixed, *before* reentering the laser, with an identical strength local oscillator. The laser parameters are identical to those in [1] and [2] and are briefly summarized here: we use a double-ended argon-ion (Ar^+) laser with a temperature-tunable intracavity étalon selecting a single longitudinal mode at 488 nm. The mirror reflectivities are approximately 95%, the axial (longitudinal) mode spacing $\Delta/2\pi$ is 156.02 MHz, and the passive mode width $\Gamma_0/2\pi$ is 2.77 MHz (FWHM) which corresponds to γ_c $(=\Gamma_0/2)$ of 8.7×10^6 s^{-1}. We define laser power (P) throughout as the output from only *one* end.

In addition to the gain measurements, we have measured intensity-fluctuation noise spectra of the laser at frequencies close to the mode spacing (156 MHz) by illuminating a fast photodiode detector (Fig. 4). The spectra are then derived by Fourier analysis of the detector output current. The noise arises from beating between the lasing mode and the emission into the two subthreshold axial modes, one on each side of the laser line. Data have been obtained for both single- and double-sideband spectra: these clearly demonstrate the existence of noise-cancellation effects. Both the gain and noise data show excellent qualitative agreement with the predictions of Sec. II; discrepancies between theory and experiment are discussed in Sec. IV.

Experiments have also been carried out in which the relative phases of the three output components (laser, signal, and image) can be varied using a Fabry-Pérot phase shifter. This allows direct examination of the PM contribution to the laser noise, and of cases intermediate between pure AM and pure PM. In addition, a "noisy" (thermal) source has been used to provide an input for the laser amplifier: the output is shown to contain two distinct noise output components in the signal and image bands. The image band noise may be considered to be the "antinoise" counterpart to the signal band noise,

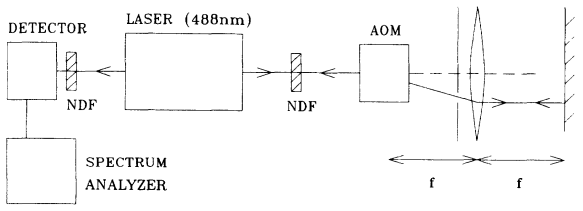

FIG. 4. The experimental arrangement. For noise measurements, only the equipment to the left of the laser is required. The other components provide an input signal for the gain measurements. NDF denotes a neutral-density filter and AOM is an acousto-optic modulator.

since its presence leads to a significant reduction of the overall noise level (noise cancellation). Finally, a study has been made of some of the other spectral lines of the Ar^+ laser. The noise spectra obtained show widely differing behavior.

A. Gain measurements

In this section we summarize briefly the gain measurements obtained in Ref. [18], and compare the results with the theory of Sec. II A. Data were obtained over a wide range of laser power, and particular care was taken to ensure that the intracavity étalon was tuned precisely into resonance with the lasing mode, in order to avoid the complex effects of asymmetric tuning described in [18]. We emphasize that the overall gain measurements reported here include the effects of both signal and image components in the output laser beam. Simple experiments were also carried out in which the output was studied with a high-resolution étalon; these verified the existence of separate amplified signal and image components. However, no detailed measurements were made on the gain experienced by these individual components.

The gain profiles are symmetric Lorentzians, in agreement with (2.36), and their center shifts to higher frequency as the laser power increases. Shift and width measurements obtained for the gain are displayed in Figs. 5 and 6. Also plotted are the theoretical predictions of (2.30) and (2.31) with suitably chosen parameter values for the decay rates γ_c and $\gamma_\parallel$, and the saturation power P_s, defined as the laser power at twice threshold pumping rate ($C=2$) [2]. The dashed curves indicate the sensitivity of the fits to the value of $\gamma_\parallel$. It should be stressed that the shift of Fig. 5 does *not* originate from a change in the mode spacing Δ: the results to be presented in Sec. III B

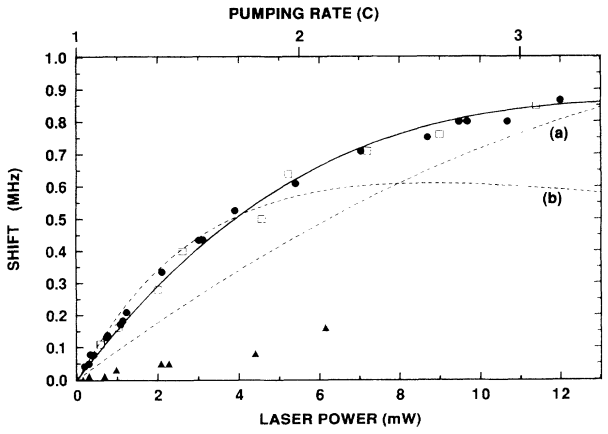

FIG. 5. Experimental values of double-sideband shift on the 488-nm line. ●, data from noise measurements; □, data from gain measurements. Solid curve: best fit to theory; $\gamma_\parallel=4.0\times10^8\ s^{-1}$, $\Delta/\gamma_\parallel=2.4$. Dashed curves: theory, with $\gamma_\parallel$ set equal to (a) $2.0\times10^8\ s^{-1}$ and (b) $8.0\times10^8\ s^{-1}$. Plotted for comparison with 488 nm is noise data (▲) obtained on the 5154-nm line (Sec. III E). Only the lower x axis (laser power) has significance for these data: the values of C would be significantly lower for 514 nm than those depicted on the upper x axis.

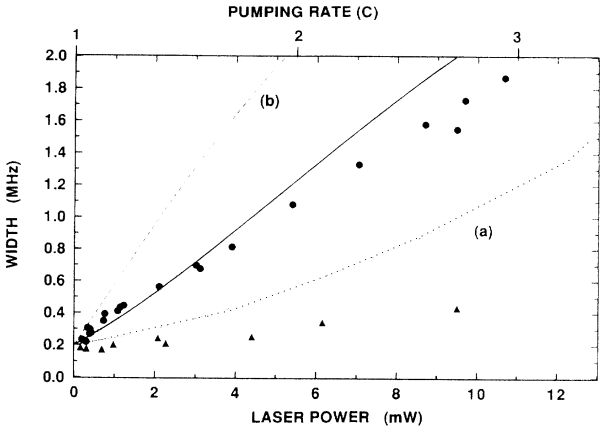

FIG. 6. Experimental values of double-sideband width. The symbols and curves refer to the same conditions as in Fig. 5.

demonstrate that Δ remains virtually unchanged as power is varied. The theory of Sec. II shows that the shift in the gain and noise profiles arises because of asymmetric cancellation of signal and image components. The cancellation effect is greater on the low-frequency side of the mode center, leading to the appearance of an overall shift of the profile to higher frequency.

Absolute values of gain were assessed by calibrating the beat gain in transmission against that in reflection at large detuning; this latter gain is assumed to be unity [2]. The product of root peak gain and bandwidth was shown to be constant to within 10%. Its independence of laser power is in agreement with (2.36). The value of the width intercept as $P\rightarrow0$ (ϵ/π) is determined by the parameters of the intracavity étalon (thickness $=11.0$ mm, refractive index $=1.47$ at 488 nm, reflectivity $=21.6\%$). The étalon is inclined slightly from the normal to the laser axis in order to avoid feedback problems. The width intercept was calculated to be 194 ± 20 kHz, in excellent agreement with observation.

B. Double- and single-sideband noise spectra

Intensity-fluctuation noise spectra were presented earlier for double-sideband [18] and single-sideband [19] detection. Here, we summarize those data and perform a more detailed analysis in order to relate the results to the theory of Sec. II B. The double-sideband measurements are the more straightforward, since they only involve detection of the total laser output, followed by Fourier analysis of the detector current. The results for shift and width are again presented in Figs. 5 and 6. The close agreement between gain and noise behavior is a particularly striking feature, emphasizing a fundamental property of amplifiers [24]. By way of contrast, the data for the 514-nm line are also plotted in Figs. 5 and 6. This line displays much reduced values of width and shift; we describe the behavior of the other Ar^+ lines in more detail in Sec. III E.

The measurements of single-sideband noise clearly reveal the noise-cancellation effects predicted in Sec. II B. In the absence of any correlation between the two noise sidebands, the single-sideband spectra would have the

same shape as for double-sideband detection, with a simple halving of the noise power level. In fact, the data show a very large *increase* in noise level for single-sideband detection. The single-sideband experiment is described in detail in [19]: one or other of the two sidebands is removed from the laser beam by filtering with a Fabry-Pérot étalon. This leaves the laser spectrum as depicted in Fig. 1(b). The measured intensity-fluctuation noise then results from a simple beat between the broadband noise component and the (effectively monochromatic) lasing mode, acting as local oscillator.

Single- and double-sideband noise spectra are shown in Fig. 7 for a range of laser power levels. At the lowest power, close to threshold, the four-wave-mixing process is weak, and so there is very little correlation between the sidebands. Under these conditions, the single-sideband noise spectrum may be obtained by simply halving that for the double-sideband measurements. However, as the laser pumping rate (C) increases, the noise cancellation quickly becomes apparent: at $C=2$, the two noise levels at frequency $\omega=\Delta$ already differ by over an order of magnitude.

The theory of Sec. II suggests that the asymmetric single-sideband noise profiles may be separated as the sum of the two Lorentzians shown in (2.49). One of these (the AM part) should have the same width and shift as the double-sideband spectrum shown in (2.54) for $\phi_E=0$, but reduced in height by a factor of 4. The PM part should contribute a component of constant width, always positioned at the mode center. At higher laser powers, it is this PM contribution that dominates. A detailed analysis confirms that the experimental profiles are consistent with this picture. Figure 8 shows an example in which the AM and PM parts have been separately

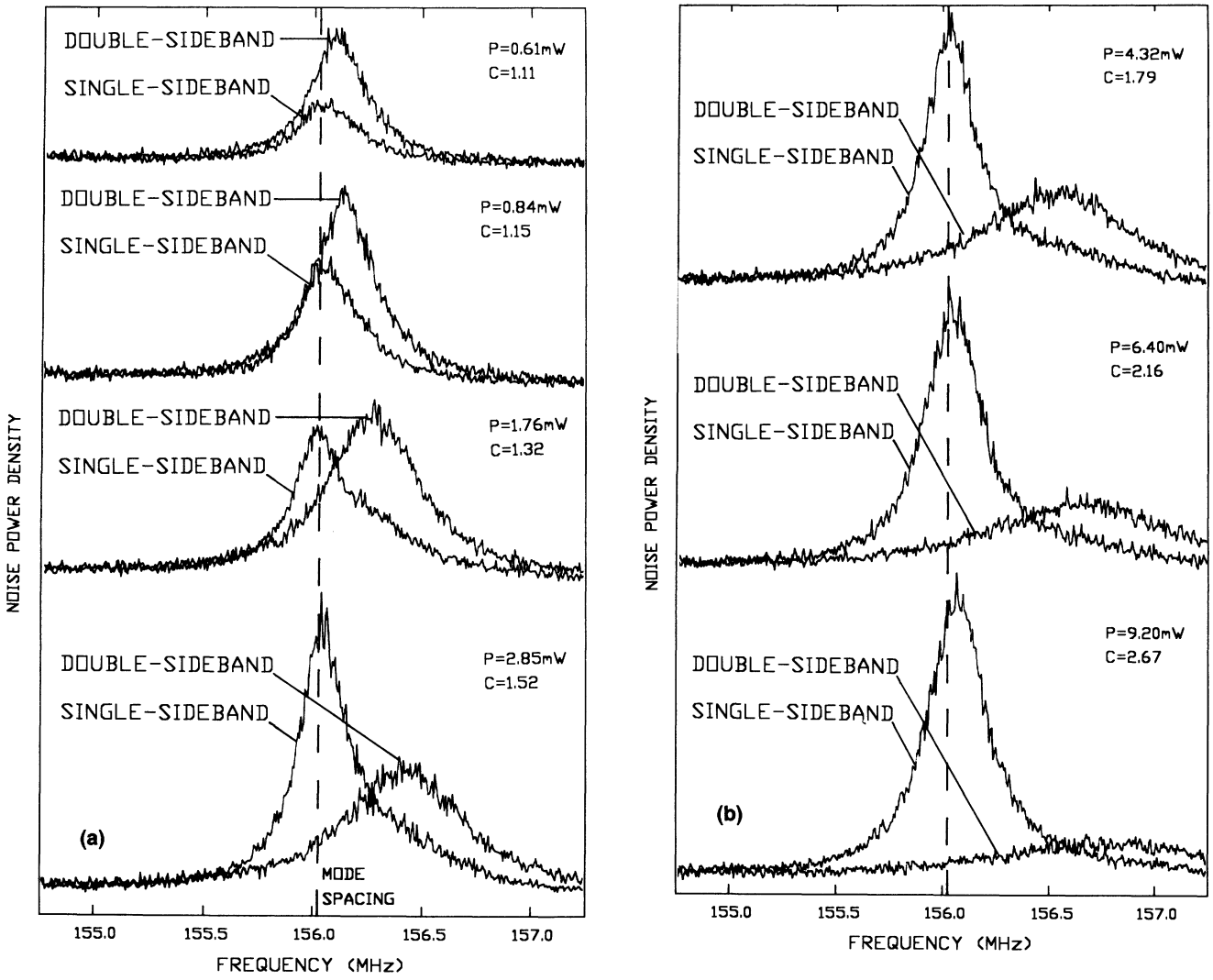

FIG. 7. Single- and double-sideband noise spectra. The noise power density is plotted on a linear scale in arbitrary units: (a) low laser power; (b) high laser power.

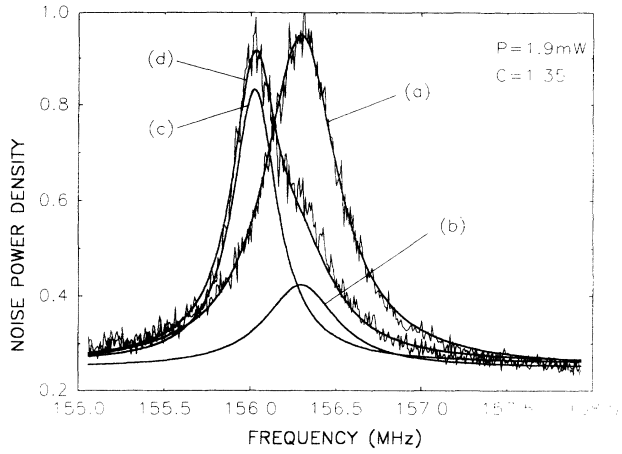

FIG. 8. Separation of single-sideband noise data (plotted on a linear scale in arbitrary units) into AM and PM components. Curve (a) represents the best fit to the double-sideband data; curve (b) is curve (a) divided by 4 and represents the AM contribution to the single-sideband spectrum [see Eqs. (2.67) and (2.68)]. The best fit to the single-sideband data [curve (d)] is the sum of two Lorentzian contributions from the AM and PM components [curves (b) and (c), respectively]. Note that the background has been subtracted from the data before fitting.

identified. The width of the PM contribution is plotted in Fig. 9 as a function of laser power. Possible reasons for its slight increase will be discussed in Sec. IV.

C. Experiments with Fabry-Pérot phase shifter

The relationship between AM and PM contributions to the noise was further explored by examining the double-sideband spectra while varying the relative phase of the three components with a Fabry-Pérot phase shifter [25,26]. This device is the same as that used for filtering out a single sideband in Sec. III B, except that one of the mirrors is of nearly 100% reflectivity. A light beam incident upon the mirror at the other end (reflectivity 89%) must now be totally reflected by the étalon, and it will acquire a phase shift up to a value of $\pm\pi$ depending on its frequency relative to the Fabry-Pérot resonance. Thus,

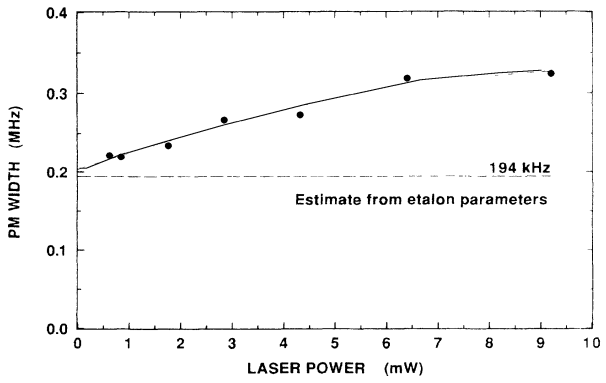

FIG. 9. Analysis of single-sideband profiles: PM width against laser power.

by tuning the étalon to alter the phase ϕ_E of the central lasing component, the noise may be cycled from pure AM far from resonance ($\phi_E=0$), through pure PM ($\phi_E=\pi/2$), and back to pure AM precisely on resonance in accordance with (2.54), (2.67), and (2.68). Figure 10 illustrates noise profiles for the pure AM and PM cases. For intermediate phase shifts, the transition from a broadened, shifted Lorentzian (AM) to a narrow, unshifted Lorentzian (PM) is clearly apparent. No detailed measurements were carried out on these profiles because the lack of active étalon locking led to problems of long-term stability.

D. Generation of "optical antinoise"

The observation of correlated signal and image components in our laser output suggests that if a broadband ("noisy") input is injected into the laser, then the output should contain not only an amplified version of the input, but also an anticorrelated ("antinoise") component in the image band. The input noise bandwidth would obviously have to lie within the above-threshold amplifier gain bandwidth, and the effect of noise cancellation would be most noticeable at higher laser powers. We have performed such an experiment to generate optical antinoise and have achieved a large reduction in noise level when this antinoise component is detected, compared to the case when it has been eliminated by optical filtering.

The broadband input with Gaussian statistics is provided by scattering the laser beam from a rotating ground-glass screen [27]; it is tuned close to resonance with the subthreshold mode ($\omega\sim156$ MHz) by an acousto-optic modulator (as in Fig. 4, with the ground-glass screen replacing the mirror). Figure 11 shows a plot of the resulting noise measured for a laser power of about 30 mW. This power level ensures strong four-wave mixing and a high degree of correlation between output signal ("noise") and image ("antinoise") components. The effects of this correlation are clearly illustrated in Fig. 11, in which the lower trace shows the noise spectrum for the light output with no filtering. In the upper trace, the relative phase of the "noise" and "antinoise" has been altered by π with the Fabry-Pérot phase shifter, such that their contributions now add. This leads to a noise level increase of nearly two orders of magnitude, illustrating the efficiency of the noise cancellation in the original (unfiltered) output.

E. Other spectral lines of the argon-ion laser

All the experiments described so far have studied the highest gain (488 nm) spectral line of the Ar^+ laser. Because its gain is much higher than for the other lines, the blue 488-nm line provides the only lasing component at relatively low discharge currents ($I<18$ A), even when the laser employs no means of spectral selection. We have carried out experiments in which a prism is inserted into the cavity, to allow selection of the other spectral lines at appropriate values of discharge current. Measurements have been made of intensity-fluctuation noise spectra for four other lines of the Ar^+ laser. Widely

TABLE I. Relaxation rates for different spectral lines of the Ar^+ laser and corresponding lifetimes ($\tau = 1/\gamma_\parallel$) of the upper lasing level. The uncertainty in the measurement for 488 nm is about ±10%. It is ±30% for the other lines, except 514 nm, which has a small shift and as a result is subject to an uncertainty of > ±50%.

Quantity \ λ (nm)	457.9	476.5	488.0	496.5	514.5
$\gamma_\parallel$ (10^8 s^{-1})	3.1	3.3	4.0	3.5	2.8
τ (ns)	3.2	3.0	2.5	2.8	3.6
τ (ns) (from [28])	8.8	9.4	9.1	9.8	7.5

differing behavior is observed, reflecting the different saturation and relaxation rates involved for the various levels and also the sensitivity of the spectra to these rates. The measurements allow estimates to be made of the values of $\gamma_\parallel$ for each of the lasing transitions.

The cavity length is increased approximately 4% by the introduction of the frequency-selecting prism. As a result, the longitudinal-mode spacing is reduced by the same factor to between 150.25 and 150.6 MHz, depending on the wavelength of the selected lasing line. Double-sideband noise data were taken for the lines at 458, 476, 497, and 514 nm over a range of laser power, with particular attention being paid to the low powers. The various lines display significant differences in their behavior, resulting from different values of saturation power and relaxation rate, $\gamma_\parallel$. From these data, estimates were made for each spectral line of the gradient of plots of width and shift versus power in the limit of zero power (see Figs. 2, 3, 5, and 6). The values of $\gamma_\parallel$ were found from (2.34) with the pumping rate C taking a value close to 1 at low power:

$$\frac{\Gamma - 2\epsilon}{2S} = \frac{C\gamma_\parallel}{\Delta} \ . \tag{3.1}$$

Hence, this may be rewritten in the low-power limit as

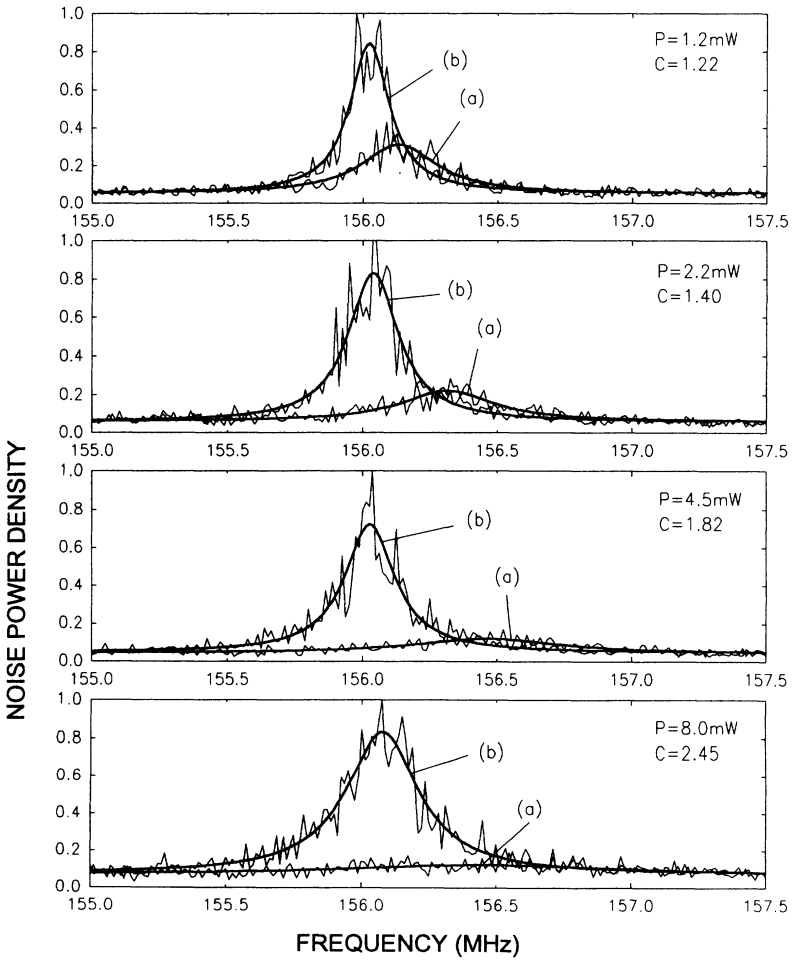

FIG. 10. Noise profiles with phase shifter (plotted on a linear scale in arbitrary units). Profiles (a) represent the noise spectrum for the natural laser output. For the profiles (b), the phase of one of the noise sidebands has been shifted by π.

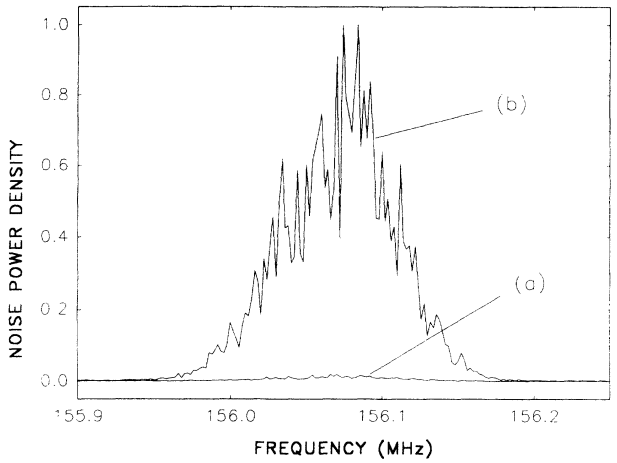

FIG. 11. Generation of optical antinoise. A noise input is injected into the laser, and the output then has "noise" and "antinoise" components in the signal and image bands, respectively. As the name suggests, these components cancel efficiently in the laser output (a). However, the noise level may be greatly increased by altering the relative phases of the components (b). The noise power density is plotted on a linear scale in arbitrary units.

$$\gamma_{\parallel}=\frac{[\text{width gradient } (P\rightarrow 0)]}{[\text{shift gradient } (P\rightarrow 0)]}\frac{\Delta}{2}\ . \tag{3.2}$$

One of the more striking features in the data is the considerably higher value of saturation power for the 514-nm line, that is, its output at twice the threshold pumping rate is about 3–4 times that for 488 nm. Width and shift data for the 514-nm line are plotted for comparison in Figs. 5 and 6. The results of the relaxation rate measurements are presented in Table I; they differ significantly from those in [28] measured by time-resolved detection of fluorescence after pulsed excitation. Indeed, our values of $\gamma_{\parallel}$ would imply decay time scales that are smaller than the experimental time resolution of [28]. Our results are not necessarily inconsistent with those of [28], since the latter work measures the free ion lifetime, whereas ours are appropriate to the rather hostile environment of the argon discharge. Hence, some of the discrepancies in Table I may arise from effects such as collisional deexcitation of ions in our discharge.

IV. DISCUSSION AND CONCLUSIONS

The work on gain and noise associated with the subthreshold modes of a laser amplifier reported in the present paper forms a natural extension of our previous study of the gain and noise associated with the lasing mode itself [2]. The theory developed in this previous work identified strong anticorrelations between the contributions to both gain and noise from frequency components within the laser line that are offset from line center by equal amounts on either side, denoted "signal" and "image" components. The anticorrelations are a consequence of pulsations in the population inversion that couple the signal and image components via a four-wave-mixing process. However, we were not able to test the theoretical predictions by experiment since the lasing line of our available argon-ion system is too narrow for practical discrimination of frequencies within the line but on opposite sides of line center. The self-heterodyne measurements that can be made with the system thus record a superposition of signal and image contributions whose separate effects cannot be unscrambled. By contrast, it should be noted that linewidths in semiconductor laser systems are typically many orders of magnitude greater than in gas lasers, allowing experimental studies of the light obtained by filtering frequency components within the laser line [29,30].

The experimental difficulties associated with the laser line in the argon-ion system are overcome in the work reported in the present paper, by shifting attention to the adjacent subthreshold modes on either side of the lasing mode. The theoretical description of the three longitudinal modes that must now be considered is somewhat more complicated, but the same anticorrelation effect, mediated by population pulsation and four-wave mixing, persists as the detuning increases from the confines of the central laser line to the next adjacent modes on either side. The three modes are sufficiently well separated for their contributions to be filtered individually by Fabry-Pérot techniques. Comparisons of the measured gain profiles and noise spectra obtained for the single adjacent modes with those obtained for the two modes in superposition clearly show the cancellation effects produced by their anticorrelations. The level of agreement between theory and experiment is generally excellent, as is particularly demonstrated by the comparisons shown in Figs. 5, 6 and 8.

We now address the discrepancies between theory and experiment; in particular, there are two effects still needing proper explanation and we suggest some possible causes. First, the measured widths of the double-sideband spectra seem too *small* at higher laser powers (Fig. 6). Second, the widths of the PM contribution to the single-sideband spectra become too *large* at the higher powers (Fig. 9), rather than remaining at a constant value as the theory predicts.

The theory throughout this paper has assumed perfect spatial homogeneity of the gain medium, and also a flat gain spectrum for the lasing medium (since $\gamma_{\perp}\gg\Delta$). These approximations are likely to break down to some extent, particularly at higher laser powers. In particular, in making the adiabatic approximation (2.11), our theory ignores any terms of a lower order in $\gamma_{\perp}$. Castelli, Lugiato, and Pirovano [31] have included such terms in a theory of frequency conversion by four-wave mixing for light injected into a laser cavity. Their results indicate that the extra terms may be of sufficient importance to explain at least partially some of the discrepancy between our theory and experiment. Dealing now with any alteration of the gain profile with laser power, spectral hole-burning effects are likely to be small, because the homogeneous broadening width is much greater than the mode spacing (see Sec. I). On the other hand, the phenomena studied here are likely to be quite sensitive to these effects, although it would be very difficult to make a

quantitative assessment of the degree of spectral hole burning. There are two aspects of spatial hole burning which must be considered in detail: namely, those due to longitudinal and transverse effects. The standing wave formed by the light field in the laser cavity possesses many minima and maxima along its axis (nodes and antinodes), separated by $\lambda/2$. The excited ions, however, are moving sufficiently quickly to "wash out" any effect of spatially dependent saturation caused by the longitudinal field inhomogeneity. A more serious discrepancy is likely to arise from the neglect in our theory of the transverse inhomogeneity of the gain medium. In reality, the intracavity field will saturate more effectively the central regions of the transverse gain distribution. At sufficiently high pumping rates, this eventually encourages higher-order transverse modes to exceed the lasing threshold, since they can make better use of the relatively unsaturated gain in the outer regions of the discharge. Inclusion of these effects may lead to a modification and distortion of the lasing mode field, which will consequently affect the gain and noise behavior studied here. The theory is currently being extended to include transverse inhomogeneities in order to describe the behavior of subthreshold transverse modes [32].

There are a number of other complications in the physics of the Ar^+ discharge that have not been included in the theory of Sec. II. We have ignored any effect due to the net ion drift velocity, typically of order 100 $m\,s^{-1}$ [33]. It would be necessary to take this drift into account in any rigorous assessment of spatial and spectral hole burning. The population of the lower level involved in the lasing transition has been assumed to be negligible throughout (perfect inversion). A nonzero lower-level population was shown in the Appendix of [2] to have a significant influence on the gain and noise spectra of Class-*B* lasers. In contrast, the gain behavior for the lasing mode of Class-*A* lasers such as Ar^+ was shown to be unaffected, and the noise was simply increased by a constant factor. However, it is not clear whether any correction for lower-level population is necessary for the situation dealt with in this paper.

We have emphasized the similarities between the anticorrelation effects that occur for pairs of signal and image components within the same central laser line and within the separated adjacent modes on either side. As was mentioned in Sec. I, higher-order transverse modes occur as satellites on the high-frequency sides alone of their lowest order (TEM_{00}) partners, and they lack the twins that are needed for the formation of anticorrelated pairs. Nevertheless, study of the gain and noise associated with the transverse modes provides both interesting contrasts with the phenomena examined here, and further insight into the mechanisms of laser action. Theoretical and experimental work on the transverse mode gain and noise in the argon-ion laser will be reported in a subsequent publication [32].

ACKNOWLEDGMENT

C.J.S. is funded by a Ministry of Defence research agreement with the University of Essex.

APPENDIX: SPECTRAL ANALYSIS OF SIGNAL AND NOISE PHOTOCURRENTS

In this appendix we wish for completeness to establish that the method of spectrum analysis employed in the experiments described leads to the quantities computed for both the gain (or signal) and the noise. For this we shall use a simplified model of the spectrum analyzer described in [34]; however, our analysis addresses different issues from those in this reference. The spectrum analyzer is assumed to perform the following sequence of operations.

(i) The (real) photocurrent $i(t)$ to be analyzed passes initially through a dc blocking filter, in which zero-frequency components are removed.

(ii) The emerging current then passes through a bandpass filter of width γ, and centered on frequency ω. The filter scans slowly through different values of ω. (Alternatively, a bank of identical-width filters could be employed, with each filter centered on a different value of ω.)

(iii) The filtered current undergoes nonlinear processing (assumed here to be the squaring operation).

(iv) The squared current is time averaged over a suitably long period T.

(v) The mean-squared signal is measured and displayed for each value of ω.

We shall consider both discrete line spectrum inputs, of the form

$$i(t)=\sum_n a_n \cos(\omega_n t-\theta_n) \quad (a_n \text{ real},\ \omega_n>0) \tag{A1}$$

(in which the a_n and ω_n are to be estimated), and continuous line spectrum inputs $i(t)$, which are assumed to be both stochastic and stationary.

The scanning filter is required to be real and causal. The simplest filter impulse response is

$$f(t;\omega)=\gamma\theta(t)e^{-\gamma t}\cos(\omega t+\phi)\ , \tag{A2}$$

in which $\theta(t)$ is the unit step function and where the scaling factor γ ensures a unit amplitude output for a unit amplitude input. The output of the scanning filter is given by

$$i_{\text{out}}(t;\omega)=\int_{-\infty}^{\infty} dt' f(t-t';\omega)i(t')\ . \tag{A3}$$

The modulation transfer function (MTF) $f(\Omega;\omega)$ of the filter is defined as the Fourier transform of the impulse response $f(t;\omega)$,

$$f(\Omega;\omega)=\frac{1}{\sqrt{2\pi}}\int_{-\infty}^{\infty} dt\, f(t;\omega)e^{i\Omega t}\ , \tag{A4}$$

and it assumes the form

$$f(\Omega;\omega)=\frac{1}{\sqrt{2\pi}}\frac{1}{2}\left[\frac{e^{i\phi}}{\gamma-i\omega-i\Omega}+\frac{e^{-i\phi}}{\gamma+i\omega-i\Omega}\right]\ . \tag{A5}$$

The filter output for the line spectrum input of Eq. (A1) is

$$i_{\text{out}}(t;\omega)=\frac{\sqrt{2\pi}}{2}\sum_n a_n\{f(\omega_n;\omega)e^{-i\omega_n t+i\theta_n} + f^*(\omega_n;\omega)e^{i\omega_n t-i\theta_n}\}\ . \tag{A6}$$

The displayed output from the spectrum analyzer is

$$O(\omega)=\lim_{T\to\infty}\frac{1}{2T}\int_{-T}^{T}dt' i_{\text{out}}^2(t';\omega)\ , \tag{A7}$$

and it takes the form

$$O(\omega)=\pi\sum_n a_n^2|f(\omega_n;\omega)|^2\ . \tag{A8}$$

It may be demonstrated straightforwardly that, for $\omega\gg\gamma$,

$$|f(\omega_n;\omega)|^2\simeq\frac{\gamma^2}{8\pi}\left[\frac{1}{(\omega-\omega_n)^2+\gamma^2}+\frac{1}{(\omega+\omega_n)^2+\gamma^2}\right]\ , \tag{A9}$$

so that

$$\lim_{\gamma\to 0}|f(\omega_n;\omega)|^2=\frac{1}{8\pi}(\delta_{\omega,\omega_n}+\delta_{\omega,-\omega_n})\ , \tag{A10}$$

where

$$\delta_{\omega,\omega_n}=\begin{cases}0, & \omega\neq\omega_n\\ 1, & \omega=\omega_n\ .\end{cases} \tag{A11}$$

In this limit it is seen from (A8) and (A10) that $O(\omega)$ does indeed reproduce the spectrum of $i(t)$, with the nth line of the spectrum having a height proportional to a_n^2.

The same apparatus is used to measure the noise power spectra. In this case an *ensemble* mean-square average of the scanning filter input gives

$$\begin{aligned}O(\omega)&=\langle i_{\text{out}}^2(t;\omega)\rangle\\ &=\int_{-\infty}^{\infty}d\omega_1\int_{-\infty}^{\infty}d\omega_2 f(\omega_1;\omega)f(\omega_2;\omega)\\ &\quad\times e^{-i(\omega_1+\omega_2)t}\langle i(\omega_1)i(\omega_2)\rangle\ ,\end{aligned} \tag{A12}$$

where $i(\omega)$ is the Fourier transform of $i(t)$. Hence,

$$O(\omega)=\sqrt{2\pi}\int_{-\infty}^{\infty}d\omega_1|f(\omega_1;\omega)|^2c(\omega_1)\ , \tag{A13}$$

where $c(\omega)$ is the Fourier transform of $\langle i(t)i(0)\rangle$ and is the true photocurrent spectrum to be determined. In this case, however, the required continuous spectrum $c(\omega)$ is obtained in the limit

$$\lim_{\gamma\to 0}\frac{1}{\gamma}O(\omega)=\frac{\sqrt{2\pi}}{4}c(\omega)\ , \tag{A14}$$

since $|f(\omega;\omega_1)|^2/\gamma$ is a density, with the asymptotic value

$$\lim_{\gamma\to 0}|f(\omega;\omega_1)|^2/\gamma=\tfrac{1}{8}[\delta(\omega-\omega_1)+\delta(\omega+\omega_1)]\ , \tag{A15}$$

and $c(\omega)$ is an even function of ω. From Eqs. (A8) and (A14) it appears that a factor proportional to the scanning filter bandwidth γ distinguishes continuous power spectra from discrete line spectra in the spectrum analyzer output. When the removal of zero-frequency components in $i(t)$ is taken into consideration, it is clear from this discussion that the ideal noise spectrum measured by the detector is proportional to $s(\omega)$, where

$$s(\omega)=\int_{-\infty}^{\infty}dt\, e^{i\omega t}\{\langle|\alpha(t)|^2|\alpha(0)|^2\rangle-\langle|\alpha(0)|^2\rangle^2\}\ , \tag{A16}$$

in which the photocurrent $i(t)$ has been assumed to be proportional to the instantaneous detected field intensity $|\alpha(t)|^2$. The complete noise spectrum also contains a constant additive shot-noise component; see [35] for a complete derivation.

As an example of the detection of line spectrum signals, consider the case of a cavity field consisting of a strong mode at frequency ω_L, amplitude α_L, and two weak modes of amplitude α_+ and α_- equally spaced on either side. The detected field, measured outside the cavity, is a continuous mode field equal to the total internal field $\alpha(t)$, scaled by the cavity lifetime factor $\gamma_c^{1/2}$. It is thus proportional to

$$\begin{aligned}\gamma_c^{1/2}\alpha(t)=\gamma_c^{1/2}(&\alpha_L e^{-i\omega_L t}+\alpha_+ e^{-i\omega_L t-i\Delta t}\\ &+\alpha_- e^{-i\omega_L t+i\Delta t})\ ,\end{aligned} \tag{A17}$$

with

$$\alpha_\pm\ll\alpha_L\ . \tag{A18}$$

To order $|\alpha_\pm|$, the photocurrent $i(t)$, proportional to $|\alpha(t)|^2$, will be

$$i(t)=k\gamma_c(|\alpha_L|^2+Ae^{-i\Delta t}+A^*e^{i\Delta t})\ , \tag{A19}$$

where k is some constant and

$$A=\alpha_L\alpha_-^*+\alpha_L^*\alpha_+\ . \tag{A20}$$

The zero-frequency term $k\gamma_c^{1/2}|\alpha_L|^2$ is blocked by subsequent processing, and the spectrum analyzer receives the current

$$i(t)=2k\gamma_c|A|\cos(\Delta t-\chi)\ , \tag{A21}$$

where

$$A=|A|e^{i\chi}\ . \tag{A22}$$

From the discussion above, the ideal spectrum analyzer displays a line at $\omega=\Delta$ of height proportional to $|A|^2$, and this is therefore the quantity employed for gain calculations in (2.35), and in previous publications [1,2,7,18,19]. It is clear that in the absence of either side mode α_+ or α_-, this result carries through, with an obvious modification of A in (A20). As explained in Sec. III, the signal gain is defined as the photocurrent beat amplitude for the self-beating laser output divided by the photocurrent beat amplitude which would be obtained by straightforward heterodyne mixing of the unamplified signal field β_{in} with the central laser mode output $\gamma_c^{1/2}\alpha_L\exp[-i\omega_L t]$. This latter beat amplitude is proportional to $k^2\gamma_c|\beta_s|^2|\alpha_L|^2$, while, from the discussion above, the self-beating laser output photocurrent beat amplitude is proportional to $k^2\gamma_c^2|A|^2$. These quantities are used in the definitions (2.26), (2.27), and (2.35).

The computed noise spectrum can also be explored in more detail. With $\alpha(t)$ given by (2.37), the measured noise spectrum given in (A16) can be reduced (after dropping terms of order $|\delta\alpha|^3$ and higher) to

$$s(\omega)=\int_{-\infty}^{\infty}dt\, e^{i\omega t}\langle B(t)B(0)\rangle\ , \tag{A23}$$

where

$$B(t)=\delta A(t)e^{-i\Delta t}+\delta A^*(t)e^{i\Delta t} \tag{A24}$$

and $\delta A(t)$ is given by

$$\delta A(t)=\alpha_L^*\delta\alpha_+(t)+\alpha_L\delta\alpha_-^*(t)\ . \tag{A25}$$

In terms of $\delta A(\omega)$ [the Fourier transform of $\delta A(t)$], the noise spectrum becomes

$$s(\omega)=\frac{1}{2\pi}\int_{-\infty}^{\infty}d\omega'\langle[\delta A(\omega)+\delta A^*(-\omega)] \times[\delta A(\omega')+\delta A^*(-\omega')]\rangle\ . \tag{A26}$$

In Sec. II only the quantities of the form $\langle\delta A(\omega)\delta A^*(\omega')\rangle$ have been calculated (with the additional phase shift ϕ_E). A calculation which includes the contributions of $\langle\delta A(\omega)\delta A(\omega')\rangle$ and $\langle\delta A^*(\omega)\delta A^*(\omega')\rangle$ gives (for zero phase shift ϕ_E)

$$s(\omega)=\frac{1}{2\pi}4\gamma_c|\alpha_L|^2\left\{\left|\frac{-i\Delta+\gamma_\parallel}{h(\omega,\Delta)}+\frac{i\Delta+\gamma_\parallel}{h(\omega,-\Delta)}\right|^2 +\gamma_\parallel^2(C-1)\left|\frac{1}{h(\omega,\Delta)}+\frac{1}{h(\omega,-\Delta)}\right|^2\right\}, \tag{A27}$$

where

$$h(\omega,\Delta)=[-i(\omega-\Delta)+\varepsilon](-i\Delta+C\gamma_\parallel)+2\gamma_c\gamma_\parallel(C-1)\ . \tag{A28}$$

Retaining only the "diagonal" terms in Eq. (A27), we find

$$s(\omega)=\frac{1}{2\pi}4\gamma_c|\alpha_L|^2\left\{\left|\frac{\mp i\Delta+\gamma_\parallel}{h(\omega,\pm\Delta)}\right|^2 +\gamma_\parallel^2(C-1)\left|\frac{1}{h(\omega,\pm\Delta)}\right|^2\right\}, \tag{A29}$$

where choice of the upper signs produces the Lorentzian centered at $\omega=\Delta+S$, corresponding to the second term in the large bracket of (2.54). The lower signs produce a Lorentzian centered at $\omega=-\Delta-S$, whose effect is negligible at the positive measured frequencies ω. The "cross" terms in (A27) correspond to autocorrelations in δA and δA^*, and they can also be shown to be small. These quantities have therefore been neglected in the treatment of Sec. II B. Finally, in the absence of either side mode field fluctuation $\delta\alpha_+$ or $\delta\alpha_-$, the theory undergoes an obvious modification following a redefinition of $A(t)$ in (A25), upon removal of the term $\delta\alpha_+$ or $\delta\alpha_-$.

[1] M. Harris, R. Loudon, G. L. Mander, and J. M. Vaughan, Phys. Rev. Lett. **67**, 1743 (1991).
[2] R. Loudon, M. Harris, T. J. Shepherd, and J. M. Vaughan, Phys. Rev. A **48**, 681 (1993).
[3] M. D. Sayers and L. Allen, Phys. Rev. A **1**, 1730 (1970).
[4] M. Sargent, M. O. Scully, and W. E. Lamb, *Laser Physics* (Addison-Wesley, Reading, MA, 1974).
[5] P. Meystre and M. Sargent, *Elements of Quantum Optics* (Springer-Verlag, Berlin, 1990).
[6] L. M. Narducci, J. R. Tredicce, L. A. Lugiato, N. B. Abraham, and D. K. Bandy, Phys. Rev. A **33**, 1842 (1986).
[7] M. Harris, R. Loudon, T. J Shepherd, and J. M. Vaughan, Opt. Commun. **101**, 432 (1993).
[8] M. Brambilla, F. Castelli, L. A. Lugiato, F. Prati and G. Strini, Opt. Commun. **83**, 367 (1991).
[9] S. Inoue, H. Ohzu, S. Machida, and Y. Yamamoto, Phys. Rev. A **46**, 2757 (1992).
[10] A. P. Bogatov, P. G Eliseev, and B. N. Sverdlov, IEEE J. Quantum. Electron. **QE-11**, 510 (1975).
[11] G. P. Agrawal, J. Opt. Soc. Am. B **5**, 147 (1988).
[12] M. Yamada and Y. Suematsu, J. Appl. Phys. **52**, 2653 (1981).
[13] R. F. Kazarinov, C. H. Henry, and R. A. Logan, J. Appl. Phys. **53**, 4631 (1982).
[14] M. Yamada, IEEE J. Quantum. Electron. **QE-19**, 1365 (1983).
[15] M. Sargent, S. W. Koch, and W. W. Chow, J. Opt. Soc. Am. B **9**, 1288 (1992).
[16] A. P. Bogatov, P. G. Eliseev, O. A. Kobildzhanov, and V. R. Madgazin, IEEE J. Quantum. Electron. **QE-23**, 1064 (1987).
[17] M. P. van Exter, R. F. M. Hendriks, J. P. Woerdman, and C. J. van der Poel (unpublished).
[18] M. Harris, R. Loudon, T. J. Shepherd, and J. M. Vaughan, Opt. Commun. **91**, 383 (1992).
[19] M. Harris, R. Loudon, T. J. Shepherd, and J. M. Vaughan, Phys. Rev. Lett. **69**, 2360 (1992).
[20] M. D. Levenson, W. H. Richardson, and S. H. Perlmutter, Opt. Lett. **14**, 779 (1989).
[21] M. Harris, C. A. Hill, and J. M. Vaughan, Electron. Lett. **29**, 997 (1993).
[22] W. H. Louisell, *Quantum Statistical Properties of Radiation* (Wiley, New York, 1973).
[23] A. E. Siegman, *Lasers* (University Science Books, Mill Valley, CA, 1986).
[24] C. M. Caves, Phys. Rev. D **26**, 1817 (1982).
[25] M. D. Levenson, R. M. Shelby, A. Aspect, M. Reid, and D. F. Walls, Phys. Rev. A **32**, 1550 (1985).
[26] J. M. Vaughan, *The Fabry-Pérot Interferometer* (Adam Hilger, Bristol, 1989).
[27] M. Harris, G. N. Pearson, C. A. Hill, and J. M. Vaughan, Appl. Opt. (to be published).
[28] W. R. Bennett, P. J. Kindlmann, G. N. Mercer, and J. Sunderland, Appl. Phys. Lett. **5**, 158 (1964).
[29] R. Centeno Neelen, D. M. Boersma, M. P. van Exter, G. Nienhuis, and J. P. Woerdman, Phys. Rev. Lett. **69**, 593 (1992).

[30] T. Yabuzaki, T. Mitsui, and U. Tanaka, Phys. Rev. Lett. **67**, 2453 (1991).
[31] F. Castelli, L. A. Lugiato, and R. Pirovano, Phys. Rev. A **49**, 4031 (1994).
[32] C. J. Shackleton, R. Loudon, C. A. Hill, M. Harris, T. J. Shepherd, and J. M. Vaughan (unpublished).
[33] E. A. Ballik, W. R. Bennett, and G. N. Mercer, Appl. Phys. Lett. **8**, 214 (1966); C. E. Webb (private communication).
[34] M. Lax, in *Statistical Physics, Phase Transitions and Superfluidity,* 1966 Brandeis University Summer Institute in Theoretical Physics, edited by M. Chrétien, E. P. Gross, and S. Deser (Gordon and Breach, New York, 1968).
[35] E. Jakeman and R. Loudon, J. Phys. A **24**, 5339 (1991).